Discover Oncology

Research

SELP can affect the immune microenvironment of gastric cancer and is associated with poor prognosis

Yue Wu[1] · Jingyu Liu[1] · Tong Yin[1] · Xiaoxiao Li[1] · Xian Liu[1] · Xiaobo Peng[1] · Xianbao Zhan[1]

Received: 9 January 2025 / Accepted: 8 May 2025
Published online: 21 May 2025

Abstract
The tumor microenvironment (TME) plays a crucial role in the occurrence and progression of gastric cancer. Yet, we still don't understand how immune and stromal components of TMEs are modulated. In this study, we applied the ESTIMATE algorithm to calculate the number of immune and stromal components in 410 STAD cases in the Cancer Genome Atlas (TCGA) database. COX regression analysis and protein–protein interaction (PPI) network construction were used to analyze differentially expressed genes (DEGs). Then, P-selectin (SELP) was identified as a predictor by cross-analysis of univariate COX and PPI. After verifying the clinical significance of SELP for study, we performed an immune infiltration analysis and identified 54 immunomodulators associated with SELP through public data. Immunomodulation associated with gastric cancer prognosis was then confirmed by LASSO regression, and the previous results were further validated with single-cell data. Finally, we verified that SELP can promote EMT on gastric cancer cells. In conclusion, we validated that SELP may affect the biological phenotype of gastric cancer with the immune microenvironment alteration of gastric cancer.

Keywords Gastric cancer · Tumor microenvironment · ESTIMATE algorithm · Immune · Stromal · SELP

1 Introduction

Gastric cancer (GC) is the fifth most common malignancy worldwide and the fourth leading cause of cancer-related death [1, 2]. According to data from the International Agency for Research on Cancer (IARC), there are approximately 480,000 new cases of gastric cancer in China, accounting for approximately 44% of global gastric cancer cases [2]. Although early stage gastric cancer (Tis, carcinoma in situ) responds well to treatment [3, 4], most patients are diagnosed at an advanced stage because of the limited indications and symptoms of precancerous lesions [5]. Despite the continuous iteration of comprehensive treatments based on surgical resection, the prognosis of GC remains poor, with a median survival of only 12–15 months [6, 7]. Consequently, the global burden of gastric cancer remains high, especially in Asia and Latin America [8]. There have been 370,000 gastric cancer deaths in China, accounting

Yue Wu, Jingyu Liu and Tong Yin contributed equally to this work.

Supplementary Information The online version contains supplementary material available at https://doi.org/10.1007/s12672-025-02629-6.

✉ Xiaobo Peng, pxb023@126.com; ✉ Xianbao Zhan, zhanxianbao@126.com | [1]Department of Oncology, Changhai Hospital, Naval Military Medical University, Shanghai 200433, China.

for half of the world's total deaths [9]. Therefore, there is an urgent need to explore potential therapeutic targets for the treatment of GC.

More and more studies have shown that the tumor microenvironment (TME) is epigenetically related to tumor cells and plays a key role in the initiation [10], progression and metastasis of tumors [11, 12]. The immune microenvironment is crucial, and in the recruitment of tumor-related signals, various immune cells have been shown to interact with cancer cells to promote tumor development [13]. For example, in the complex environment of the TME, immune cells are more likely to have more M2 macrophages and Treg cells, but not fully mature immune cells, to exert tumor-suppressive functions [14]. Current studies have found that the response to immune checkpoint blockade (ICB) is closely related to the TME, and ICB can effectively restore the anti-tumor immune response [15–18]. For instance, Cao et al. found that SLC6A6-mediated taurine uptake transactivates immune checkpoint genes and induces exhaustion in $CD8^+$T cell [19]. Several studies have found that PD-1/PD-L1 inhibitors can improve the cure rate of gastrointestinal malignancies [20], and that tumors with a higher mutational burden (TMB) show better immunotherapy responses [21, 22]. However, a comprehensive understanding of the molecular mechanisms underlying the immune microenvironment in gastric cancer may be the key to ensuring the success of immunotherapy. Transcriptome sequencing patterns and functional genomic analyses have revealed the roles of different cell types in TME regulation. In this paper, the ESTIMATE computational method was used in order to calculate the proportion of immune and matrix components of STAD samples in The Cancer Genome Atlas (TCGA) database, and a predictive biological indicator, SELP, was discovered. P-selectin (SELP) is a cell adhesion molecule (CAM) that is expressed on the surface of platelets, endothelial cells, and leukocytes, and mediates the initial step of immune cell penetration from the bloodstream into surrounding tissues [23]. SELP is involved in a variety of immune processes, such as platelet activation and leukocyte recruitment and function [24]. However, the function of SELP in the GC immune microenvironment remains poorly understood. Because SELP is involved in various health and disease processes, its expression and functional patterns influence tumor development and treatment. Therefore, we have conducted a comprehensive analysis of SELP and demonstrated that it may be a potential indicator of TME alterations in gastric cancer.

2 Material and methods

2.1 Data source

In this study, transcriptome RNA-sequencing data of STAD samples were downloaded from The Cancer Genome Atlas (TCGA) database (https://portal.gdc.cancer.gov/). We also used gastric cancer transcriptome and single-cell data acquired from GSE84437 and GSE167297 via the Gene Expression Omnibus (GEO) database (https://www.ncbi.nlm.nih.gov/geo/). The specimens were screened based on the clinical data.

2.2 Calculate ImmuneScore, StromalScore and ESTIMATEScore

The ESTIMATEScore, StromalScore, and ImmuneScore of the patients are calculated using the ESTIMATE R package (developed in R version 4.0.1) [25]. The immune and stromal component scores were positively correlated with the number of immune and stromal components present in the TME. The higher the score, the greater the number of immune or stromal components present in the TME.

2.3 Survival analysis

Survival analysis was performed using the survival R package based on the Kaplan–Meier formula (log-rank test). The TCGA database contains survival information for 404 patients with STAD, which was used to plot survival curves. Survival information from 433 patients in the GEO database (GSE84437) was used to plot the survival curve. In the analysis, logarithmic rank was used as a statistical significance test; $p < 0.05$ is considered significant.

2.4 Generation of differentially expressed genes

A total of 411 tumor samples were categorized as either high or low based on the median score of ImmuneScore and StromalScore. To perform differential gene expression analysis between high and low expression groups, the edgeR package with P-value < 0.01 and log2(foldchange) > 1.5 was used [26]. To visualize significant Differentially Expressed Genes (DEGs), the ggplot2 R package was used to generate a volcano plot (comparison between the high-scoring groups vs. the low-scoring groups). Moreover, a Venn diagram was constructed in order to show the significant downregulation and upregulation of DEGs.

2.5 Differential analysis of clinical data

The STAD mRNA expression profiles and corresponding clinicopathological records are available in TCGA database. These data were analyzed using the R package and compared using the Wilcoxon rank-sum or Kruskal–Wallis rank-sum test as a significance test according to the clinical stages.

2.6 Construction of PPI network

A Protein–protein Interaction (PPI) network was constructed using the STRING database (http://www.string-db.org) and analyzed using Cytoscape version 3.7.2 (The Cytoscape Consortium, San Diego, CA, USA, http://apps.cytoscape.org). The network was built using nodes with confidence in interactive relationships greater than 0.95.

2.7 Univariate and multivariate COX analysis

Univariate and multivariate Cox analyses were performed using the R package. We analyzed the expression levels of DEGs from the ImmuneScore and StromalScore using a univariate Cox model, and the top 28 DEGs were ordered according to their p-values, from small to large. SELP-related immunomodulators associated with GC prognosis of gastric cancer were also identified using forest plots after univariate and multivariate Cox analyses.

2.8 Gene set enrichment analysis

By using gene set enrichment analysis (GSEA), pathway enrichment analysis was performed using GSEA. We downloaded the C7 gene sets collected from the Molecular Signatures Database as target sets. We considered significant gene sets with NOM $p < 0.05$ and FDR $q < 0.06$.

2.9 Immune infiltration analysis

Immune deconvolution analyses were conducted using ssGSEA and the CIBERSORT [27]. The LM22 gene profile was downloaded from the CIBERSORT website, and the proportions of 22 immune cells in the 411 STAD samples were analyzed. Furthermore, using the ssGSEA algorithm, individual tumor samples were transformed into immune cell populations. Based on a previous study [28], 28 immune cell types were identified for ssGSEA.

2.10 Immunomodulators

GC-derived SELP immunomodulators were acquired from TISIDB: an Integrated repository portal for tumor–immune system interactions database (http://cis.hku.hk/TISIDB/), In order to discern how SELP contributes to anti-tumor immunity [29]. We selected immunostimulators and immunoinhibitors that were significantly associated with SELP expression (Spearman correlation test, $P < 0.05$). These SELP-related immunomodulators were subjected to GO annotation using a Web-based Gene Set Analysis Toolkit (http://www.webgestalt.org/) [30].

2.11 Least absolute shrinkage and selection operator (LASSO)

In this study, we used LASSO regression to narrow the range of prognostic genes, remove any overfitting between them, and calculate the risk scores based on the coefficients of LASSO regression [31]. A prognostic risk-scoring model for STAD

based on a linear combination of gene expression levels and regression coefficients was constructed. The formula for the risk score is: Risk score = ∑coefficents × expression levels.

2.12 Single-cell RNA-seq analysis

In order to process the scRNA-seq dataset, we utilized the "Seurat" package (developed in R version 4.3.0) [32]. After quality control, t-SNE projection was performed to dimensionally reduce the dataset, and the cells were divided into 15 clusters. We then manually annotated the cells of these 15 clusters using existing immune cell markers, labeling seven immune cells (Epithelial, T cell, B cell, Fibroblast, Myeloid cell, Endothelial cell, Mast cell). The FeaturePlot function in the Seurat package was used to map each gene. The AddModuleScore function in Seurat was used to score the genes and display them on a volcano map. A pseudo-time trajectory analysis of potential lineages and pseudo-time trajectories was conducted using the Slingshot R package.

2.13 Cell culture

The MKN-74 and MGC-803 cells were purchased from the Cell Bank of the Chinese Academy of Sciences (Shanghai, China). Cells were cultured in RPMI-1640 (Gibco) medium with 10% fetal bovine serum (FBS) (Gibco), at 37 ℃ in a humidified 5% CO2 atmosphere.

2.14 Cell proliferation experiments

MKN-74 and MGC-803 cells were seeded in 96-well plates at a density of 3000 cells per well. After the cells are adherent, different concentrations of KF38789 (the concentrations are: 0, 0.075, 0.15, 0.3, 0.625, 1.25, 2.5, 5, 20 μM) are added to them. At 24 h, 48 h, and 72 h after adding KF38789, add 10 μL of CCK-8 (Dojindo, Japan) reagent per well under dark conditions and incubate with a constant temperature for 2 h, then measure the OD value at 450 nm of each well. Thus, cell viability under different concentrations of KF38789 was calculated, and the IC50 of the drug was determined. The cells were cultured in six-well plates at a number of 1000 cells per well for a duration of 2 weeks. After 2 weeks, the colonies were fixed in 4% formaldehyde and stained with 0.25% crystal violet. Finally, the colonies were counted and visualized.

2.15 Western blot

Proteins were extracted from MKN-74 and MGC-803 cells using an immunoprecipitation (IP) assay (Beyotime, China). Equal amounts of protein samples and protein ladders were placed in 8–12% SDS-PAGE and transferred to PVDF membranes (Biosharp, China). The cells were then incubated at room temperature or with secondary antibodies in 5% skim milk for 1 h.

2.16 Wound healing assay

We used the scratch assay to test the migratory abilities of MKN-74 and MGC-803 cells. First, the cells were seeded in 6-well plates (5 × 105 cells/well), and after adherence, the cells were treated with 0.5 μM of KF38789 for 24 h. A 10 μL pipette tip was used to scratch horizontal lines into the monolayer of cells. Images were captured using an inverted microscope (magnification × 50) at 0 h, 24 h, 48 h, and 72 h.

2.17 Transwell assay

MKN-74 and MGC-803 cells migration was examined using the transwell assay. Using a 24-well Transwell plate, we added serum-free culture media (200 μL) with 5 × 105 cells to the upper chambers and 700 μL 10% FBS to the lower chambers. We add 0.5 μM of KF38789 in both the upper and lower chambers. The visual fields of eight random chambers were counted using an inverted microscope (Olympus, Tokyo).

2.18 Statistical analysis

Graphpad Prism 9.0.0 was used for the analysis. All data are presented as mean + SEM. We used Student's *t*-test to analyze the difference between two groups based on a single variable. A statistically significant P value is defined as * P < 0.05, * * P < 0.01, or * * * P < 0.001.

3 Results

3.1 The ESTIMATE score was correlated with survival and clinicopathologic stage

First, using the ESTIMATE algorithm, the TCGA-STAD gene expression profiles were analyzed to calculate the StromalScore, ImmuneScore, and ESTIMATEScore scores of the samples. TMEs with higher ImmuneScore, StromalScore, and ESTIMATEScore scores contained more immune and stromal components. We then used Kaplan–Meier survival analysis. Despite the lack of a correlation between the ImmuneScore and OS (Fig. 1A), the StromalScore and ESTIMATEScore were positively correlated with OS for STAD patients with STAD (Fig. 1B, C). Furthermore, we analyzed the ImmuneScore, StromalScore, and ESTIMATEScore of TCGA-STAD patients with different clinicopathological characteristics. The ImmuneScore, StromalScore, and ESTIMATEScore are significantly associated with the pathological and T stages (Fig. 1D–F). Based on these results, immune components found in the TME may positively affect the prognosis of patients with STAD.

3.2 Identification of genes related with TME

According to R/edgeR, there were 917 upregulated DEGs and 601 downregulated DEGS in the ImmuneScore group (samples with high score vs. low score) and 1588 upregulated DEGs and 757 downregulated DEGS in the StromalScore group. These volcano plots show the DEGs identified by comparing high-ImmuneScore groups to low-ImmuneScore groups, as well as high-StromalScore groups to low-StromalScore groups for the ImmuneScore and StromalScore variables (Fig. 2A). A total of 598 co-upregulated genes and 408 co-downregulated genes in the two groups are displayed in a Venn plot by intersection analysis (Supplementary Fig. 1A-B).

3.3 Intersection analysis of PPI and univariate COX regression

Among these 1006 DEGs, significant interactions between 160 genes were explored using Cytoscape software [National Institute of General Medical Sciences NIGMS, USA] based on the STRING database (Fig. 2B), and the bar plot constructed shows the top 30 genes ranked by degree (Fig. 2C). To identify the valuable prognostic DEGs, 141 DEGs were analyzed by univariate Cox regression analysis. The top 28 genes are presented in a forest plot (Fig. 2D). Finally, intersection analysis was conducted to identify the DEGs that were the top 70 nodes in the PPI network and the 141 factors in the univariate COX regression, and only six genes (CD36, CXCR4, SELP, APOH, F2, and APOA1) were identified (Fig. 2E). As there are few studies on SELP in gastric cancer, we chose SELP as the subject of this study.

3.4 The correlation of SELP expression with the survival and classification of TNM stages in STAD patients

SELP is a CAM involved in intercellular, extracellular, and extracellular matrix (ECM) interactions. In addition, SELP has been shown to play a role in tumor–host interactions and cancer immunity [30]. Based on the survival analysis, SELP expression was found to be negatively correlated with survival. Patients with high SELP expression had lower survival rates than those with low SELP expression in TCGA-STAD and GSE84437 datasets (Fig. 2F). SELP was more highly expressed in tumor samples than in normal samples (Fig. 2G). Next, SELP and clinical characteristics were analyzed. As the STAD pathological and T stages progressed, SELP expression increased significantly (Fig. 2H, I). Although SELP expression did not significantly correlate with N and M stages, it increased with STAD N and M stage progression (Fig. 2J, K).

3.5 Identification of immune-related pathways by GSEA

To better understand the immunological functions of the two groups, ESTIMATE, CIBERSORT, and ssGSEA analyses were performed. The low SELP expression group had lower immune, stromal, and ESTIMATE scores than the SELP

high-expression group (Fig. 3A, B). The CIBERSORT algorithm was used to measure the proportion of immune cells in the two groups. Memory B cells, B cell nuclei, monocytes, M2 macrophages, resting dendritic cells, and resting mast cells were positively correlated with SELP expression, whereas activated CD4+T cells, M0 macrophages, and activated mast

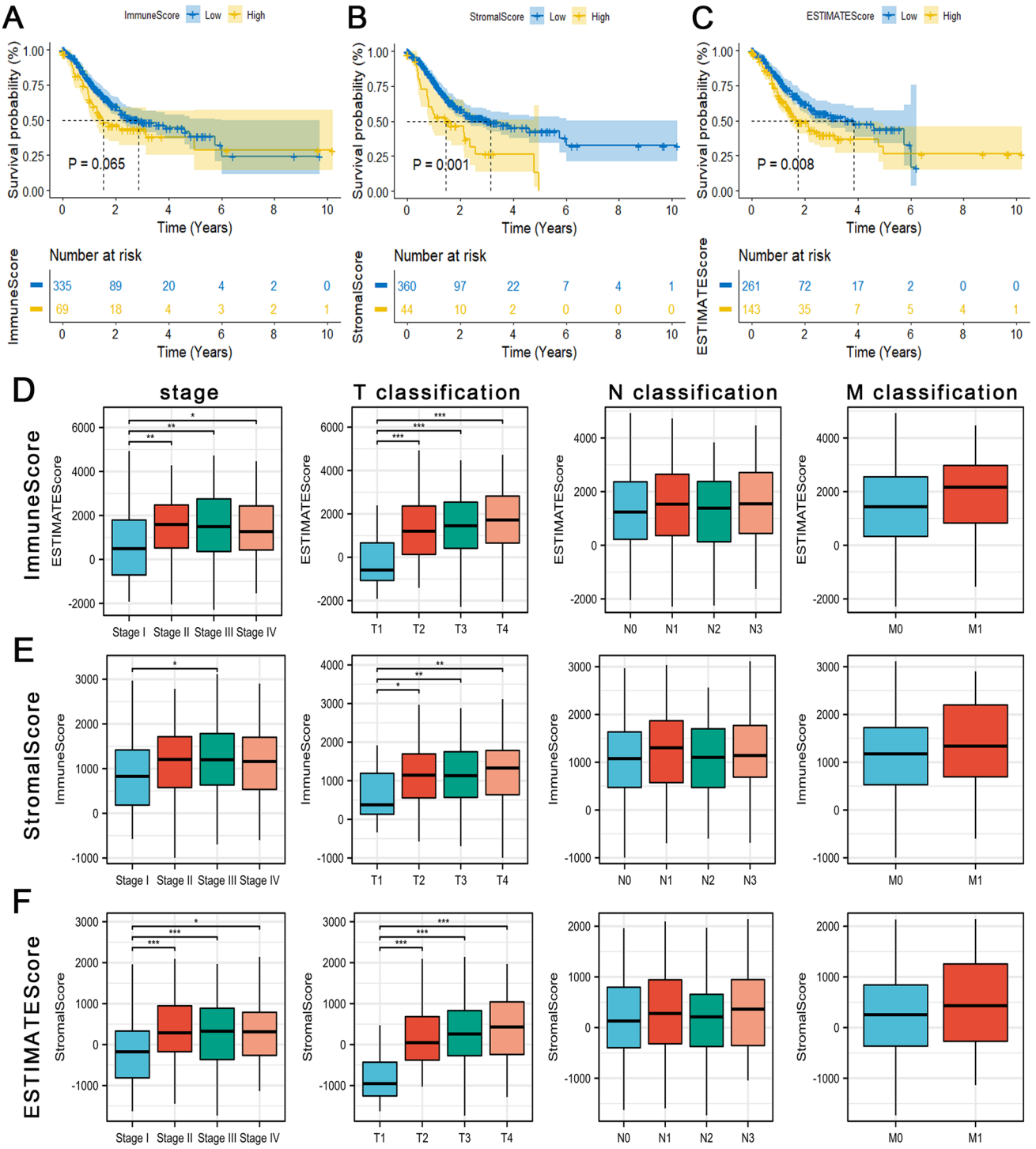

Fig. 1 Correlation of scores with clinical characteristics in patients with STAD. **A** Kaplan–Meier survival analysis of patients with STAD who are classified as high or low in the ImmunoScore (p = 0.065 by log-rank test). **B** StromalScore's Kaplan–Meier survival curve (p = 0.001 by log-rank test). **C** ESTIMATEScore's Kaplan–Meier survival curve (p = 0.008 by log-rank test). **D** Relationship between stage and TMN classification and ImmunoScore in STAD patients (*P < 0.05, * *P < 0.01, or ***P < 0.001). **E** Relationship between stage and TMN classification and StromalScore in STAD patients (* P < 0.05, ** P < 0.01, or ***P < 0.001). **F F** Relationship between stage and TMN classification and ESTIMATEScore in STAD patients (* P < 0.05, ** P < 0.01, or ***P < 0.001)

cells were negatively correlated with SELP expression (Fig. 3D). Furthermore, 28 immune cell subtypes were enriched in both groups using ssGSEA. Almost all of the immune functions were highly expressed in the SELP high-expression group (Fig. 3E). The SELP high-expression group displayed stronger immune cell infiltration than SELP low-expression group.

3.6 Comparison of immune infiltrates

To broadly understand the significance of SELP in tumor immunity, we divided the tumor samples in TCGA-STAD into SELP high-expression group and SELP low-expression group with the median level of SELP expression. An analysis of differentially expressed genes was conducted between the two groups (SELP high-expression group vs. SELP low-expression group). As soon as the DEGs were identified, we used GSEA to explore whether they were functionally enriched. Based on MSigDB's definition of the C7 collection, immunological gene sets and multiple immune functional gene sets were enriched (Fig. 3A, B).

3.7 Immunotherapy sensitivity assessment

To evaluate the sensitivity of patients with STAD to immunotherapy, we compared immune checkpoint gene expression levels between the two groups. The expression levels of multiple immune checkpoint genes differed between the SELP high- and low-expression groups. The expression levels of immune checkpoints (PD1, PDL1, PDL2, CTLA4, CD80, CD86, LAG3, TIM3, TIGHT, OX40, GITR, 4-1BB, ICOS, CD27, and CD70) were higher in the SELP-high group (Fig. 3F–I). Considering that different genetic mutations can influence the effectiveness of immunotherapy, we evaluated the mutational conditions in STAD (Supplementary Fig. 1C, D). These results suggest that STAD in the SELP high expression group may respond to immunotherapy better than STAD in the SELP low expression group.

The effects of immunotherapy can vary depending on the genetic mutations, which is why we evaluated STAD mutational conditions. Supplementary Fig. 1C, D, we depicts the mutation landscapes of the SELP high- and low-expression groups. Surprisingly, this finding was contrary to our expectations. The TMB and number of MLH1, MSH2, MSH6, PMS2, POLE, and POLD1 mutations in the SELP low expression group were higher than those in the high expression group (Supplementary Fig. 1E, F), indicating that the SELP low expression group may have a better effect on immunotherapy. This indicates that SELP plays a dual role in gastric cancer, which may be related to its involvement in normal immune function [33].

3.8 Association of SELP and immunomodulators

To determine how immunomodulators interact with SELP, we examined the impact of SELP on the immune system and the correlation between SELP expression levels and immune cell subsets. The association between STAD and lymphocytes, immunoinhibitors, and immunostimulators is shown in Fig. 4A–C. We identified 38 immunostimulators and 16 immunoinhibitors that were significantly associated with SELP in patients with STAD (Supplementary Fig. 2A, B). Next, these immunomodulatory genes were subjected to PPI network analysis (Fig. 4D). We used GO to further analyze the functions of these genes in cellular processes, metabolic processes, and biological mechanisms. These genes were also associated with primary immunodeficiency, Natural killer cell-mediated cytotoxicity, and T-cell receptor signaling pathways (Fig. 4E).

3.9 The significance of SELP-associated immunomodulators in the prognosis of STAD

To investigate the prognostic value of SELP-associated immunomodulators in patients with STAD. First, we used LASSO regression to screen for genes associated with STAD prognosis among these SELP-associated immunomodulators (Fig. 5A, B). We identified eight genes (PDCD1, TGFB1, CXCR4, IL6, TNFRSF9, TNFSF18, and TNFSF13) that were highly associated with STAD (Fig. 5C). The distributions of risk scores, outcome statuses, and gene profiles for TCGA-STAD are shown in Fig. 5D–F. Similar results were confirmed for GSE84437 (Fig. 5G–I). According to univariate Cox regression models, the risk score in TCGA-STAD was significantly associated with OS [hazard ratio (HR) = 2.077, 95% confidence interval (CI) = 1.313–3.286]. Moreover, multivariate Cox regression analysis showed that the risk score was predictive of prognosis [hazard ratio (HR) = 2.166, 95% confidence interval (CI) = 1.447–3.243] (Fig. 5J, K).

Fig. 2 Difference analyses and Correlation of SELP with clinical characteristics in patients with STAD. **A** Volcano maps generated by comparing the DEGs in the high score group and low score group in the ImmuneScore and StromalScore. The fold-change > 1 and q = 0.05 was used as the significance threshold. **B** PPI network of DEGs. An interaction network constructed by nodes with an interaction confidence value of > 0.95. **C** Barplot of top 30 genes sorted by number of nodes. **D** Univariate COX regression analysis of 141 DEGs with the top 28 significant factors of p < 0.005 were listed. **E** Venn plot showing the common factors shared by leading 30 nodes in PPI and top significant factors in univariate COX. **F** Survival analysis for STAD patients with different SELP expression in TCGA and GSE84437. **G** Differentiated expression of SELP in the normal and tumor sample. **H**–**K** Relationship between stage and TMN classification and SELP in STAD patients (*P < 0.05, ** P < 0.01, or ***P < 0.001)

3.10 Genome-wide single-cell sequencing analysis reveals the distribution of SELP in cells

In order to further clarify the role of SELP and SELP-associated immunomodulators in STAD prognosis, we performed a single-cell analysis on the GSE167297 dataset. We first performed a t-SNE projection to dimensionally reduce the dataset, and then the cells were divided into 15 clusters (Supplementary Fig. 3). We then manually annotated all clusters using the marker expression data (Fig. 6A, B). We observed a significant reduction in B cells in deep tumors by verifying the proportion of cells that had been annotated in normal tissues, superficial tumors, and deep tumors (Fig. 6C). Through the position of SELP, we found that SELP is highly enriched in endothelial cells (Fig. 6D). This is consistent with the biology of the SELP itself. Next, we used AddModulesCore to score the annotated cells with the eight prognostically relevant immune genes mentioned above. Additionally, T and myeloid cells showed relatively high scores (Fig. 6E, F). Based on the median immune score, we divided the cells into high- and low-scoring groups. The high-scoring group was mainly distributed in the T, B, and myeloid cells (Fig. 6G). Next, we built an unsupervised single-cell trajectory using Monocle on the ECs. This analysis revealed a continuous lineage path with four branches and further identified several temporal patterns of gene expression, such as IL6 and TNFRSF9, which are highly expressed early and decrease with development. PDCD1 and TGFBR1 peaked at the mid-to-late stage, and the other two genes were highly expressed at the late stage (Fig. 6H, I). These results summarized the location and development of SELP and SELP-associated immunomodulators in the TME of patients with gastric cancer. This indicates that SELP is a potential target for gastric cancer immunotherapy.

3.11 SELP promotes EMT of gastric cancer cells

To further validate these results, we found KF38789 that selectively inhibited the binding of SELP to PSGL-1. By inhibiting the function of SELP in gastric cancer cells, we investigated whether the biological functions of gastric cancer cells changed. First, we detected SELP expression in gastric cancer cell lines by western blotting. In subsequent experiments, MKN-74 cells with high SELP expression and MGC-803 cells with low SELP expression were selected (Supplementary Fig. 3C, D). The CCK8 assay was used to determine whether KF38789 regulates MKN-74 and MGC-803 proliferation. The cell viability ratio decreased with increasing drug concentration (Fig. 7A). We also derived the IC50 of KF38789 for MKN74 and MGC803 from this experiment, and finally determined the KF38789 drug concentration (0.5 μM) and the time of drug treatment (24 h). We conducted experiments to verify our conclusions using plate clone formation. Under the effect of KF38789, the colonies of MKN74 and MGC803 cells were smaller than those in the control group (Fig. 7B, C). Western blotting was performed to determine whether the protein levels of the EMT-related molecules were inhibited by KF38789. The western blot experiments showed that the levels of EMT-related proteins in gastric cancers cells changed significantly after 24 h of KF38789 treatment. Twist, N-cadherin, and vimentin expression was significantly decreased, and E-cadherin expression was significantly increased in MKN-74 and MGC-803 cells (Fig. 7D, E). Transwell and wound healing assays were performed to determine the effects of KF38789 on the migration of MKN-74 and MGC-803 cells. The results indicated that culture in KF38789 significantly decreased the migration of MKN-74 and MGC-803 cells compared to the control groups (Fig. 7F–I). These results illustrate that SELP inhibitors inhibit EMT in gastric cancer cells and they also imply that SELP promotes EMT in gastric cancer.

4 Discussion

This study has attempted to identify TME-related genes from The (TCGA) database that contribute to the survival and TNM staging classification of patients with STAD. SELP is involved in immunization Importantly, a series of bioinformatics analyses illustrated that SELP may be associated with TME status in STAD patients.

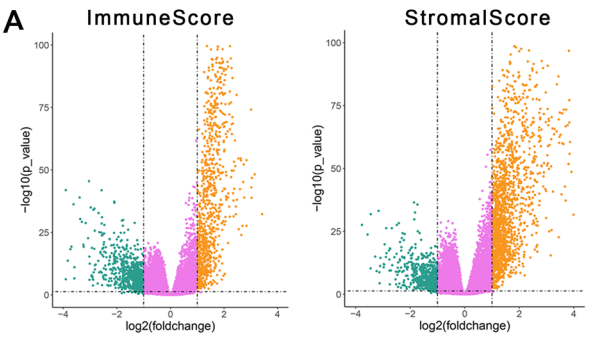

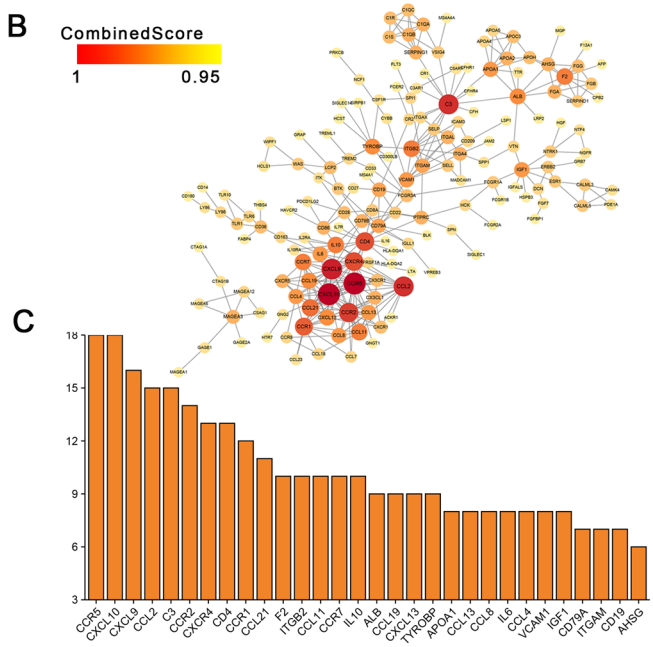

D

Gene	HR	lower 95%CI	upper 95%CI	pvalue
GDF6	1.613	1.307	1.991	0.000
CD36	1.303	1.149	1.479	0.000
ABCA6	1.541	1.249	1.902	0.000
PDE1A	1.389	1.184	1.630	0.000
EFEMP1	1.215	1.104	1.338	0.000
MMRN1	1.277	1.132	1.441	0.000
FLRT2	1.395	1.183	1.645	0.000
DCLK1	1.323	1.144	1.531	0.000
PLPPR4	1.305	1.136	1.499	0.000
H2BW1	1.678	1.274	2.212	0.000
IGFN1	1.519	1.208	1.909	0.000
UPK1B	1.149	1.065	1.241	0.000
ABCA8	1.238	1.100	1.392	0.000
SVEP1	1.239	1.100	1.394	0.000
CXCR4	1.267	1.112	1.445	0.000
CDO1	1.270	1.112	1.451	0.000
ABCA9	1.377	1.152	1.645	0.000
MEOX2	1.209	1.086	1.347	0.001
CRTAC1	1.298	1.119	1.506	0.001
CYP1B1	1.173	1.071	1.284	0.001
KCNS2	2.160	1.388	3.362	0.001
FABP4	1.145	1.059	1.238	0.001
VTN	1.130	1.053	1.212	0.001
SELP	1.211	1.083	1.353	0.001
TLL1	1.525	1.191	1.953	0.001
SYT4	1.305	1.115	1.528	0.001
ACSM5	1.968	1.318	2.937	0.001
SLIT2	1.208	1.079	1.351	0.001

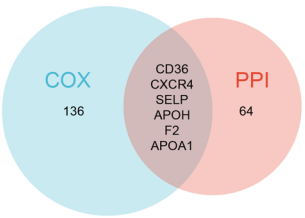

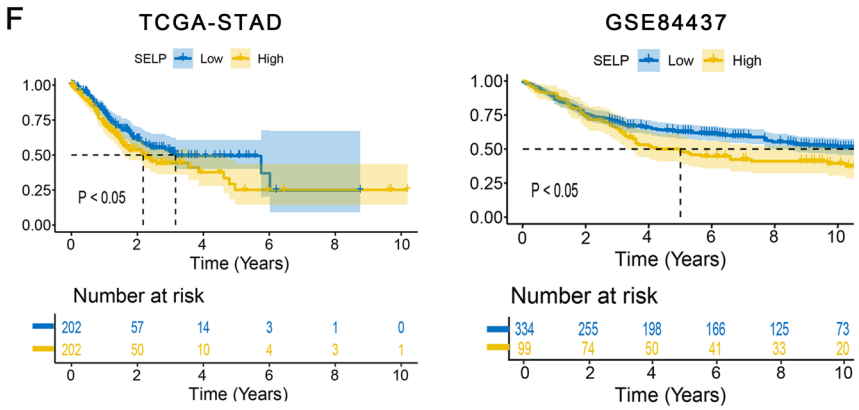

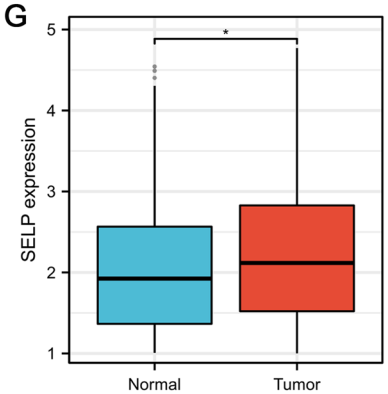

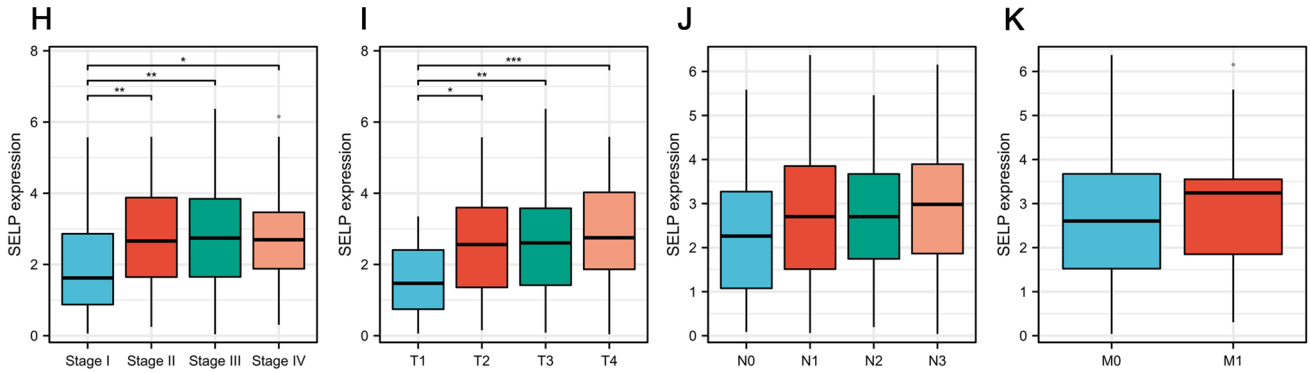

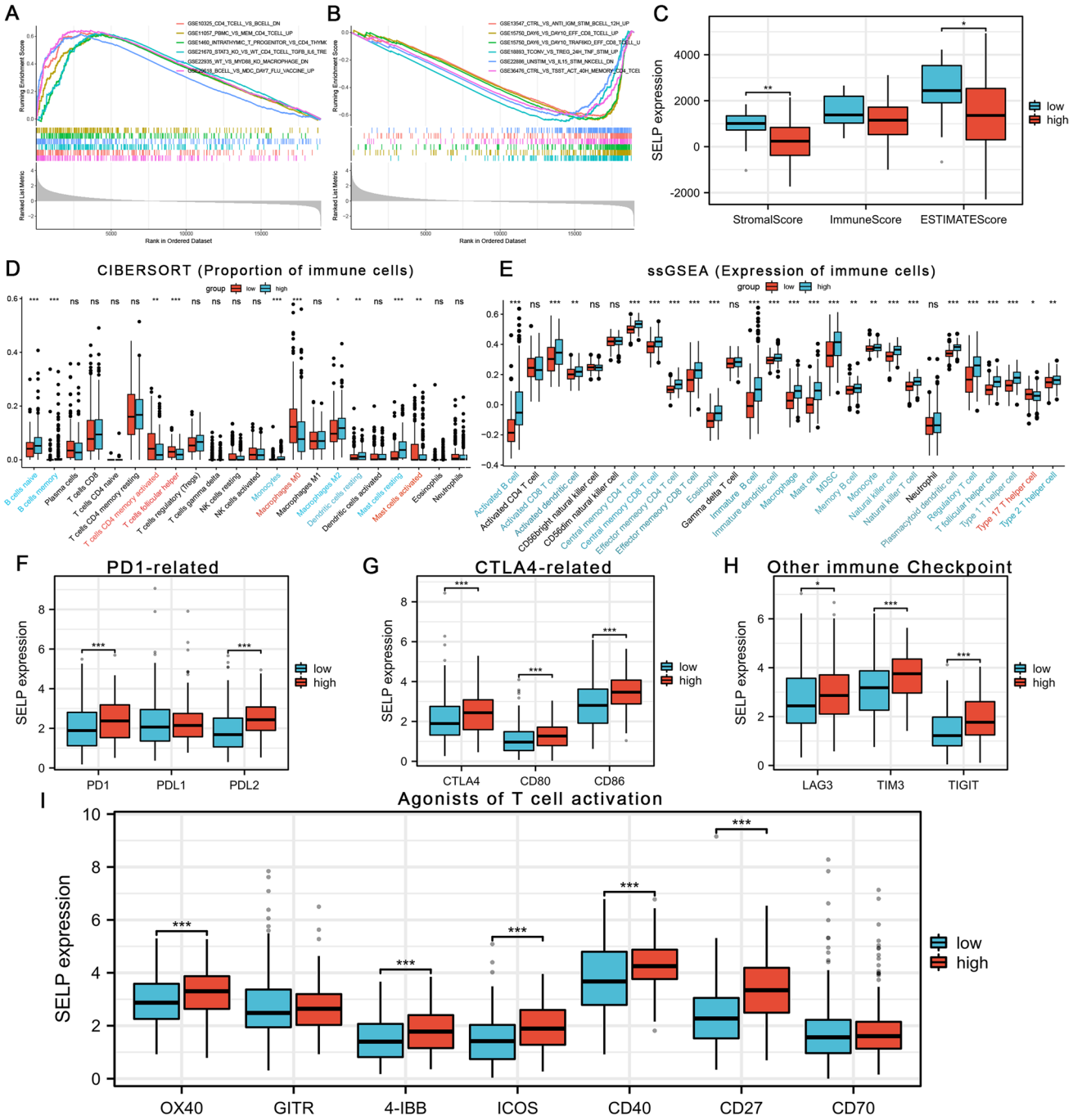

Fig. 3 Comparison of immune profiles and sensitivity to Immunotherapy between the two groups. **A** Gene enrichment analysis. On the left are pathways positively correlated to SELP, and on the right are pathways negatively correlated with SELP, each represented by a different color. **B** Comparison of ImmuneScore, StromalScore and ESTIMATEScore between SELP-high expression group and SELP-low expression group. **C** Comparison of ImmuneScore, StromalScore and ESTIMATEScore between two groups. **D** Comparison of CIBERSORT between two groups. **E** Comparison of ssGSEA between two groups. **F**–**I** Comparison of immunomodulatory drug targets between the two groups (*P < 0.05, **P < 0.01, or ***P < 0.001)

TME play a crucial role in tumor development [34]. Our transcriptome analysis of STAD data in TCGA database showed that the immune component of the TME had an adverse effect on the prognosis of patients. In particular, we found that the EstimateScore and StromalScore were significantly positively correlated with the progression (invasion and metastasis) of STAD, indicating an important interaction between immune cells and cancer cells.

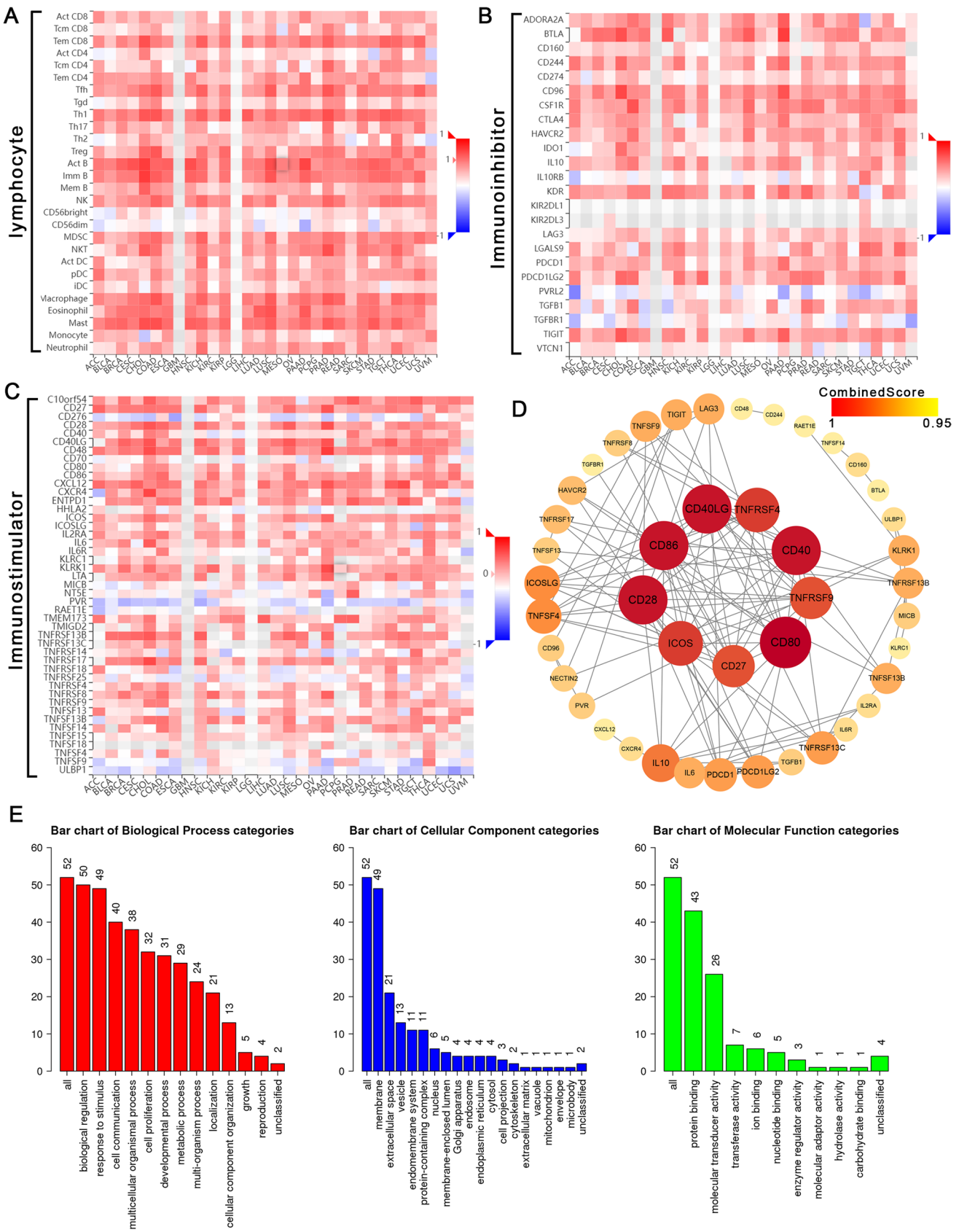

Fig. 4 Analysis of immunomodulators associated with SELP. **A** The relationship between cancers and lymphocytes. **B** The relationship between cancers and immunoinhibitors. **C** The relationship between cancers and immunostimulators. **D** PPI network of 54 immunomodulators associated with SELP. **E** GO functional analysis of SELP-related immunomodulators

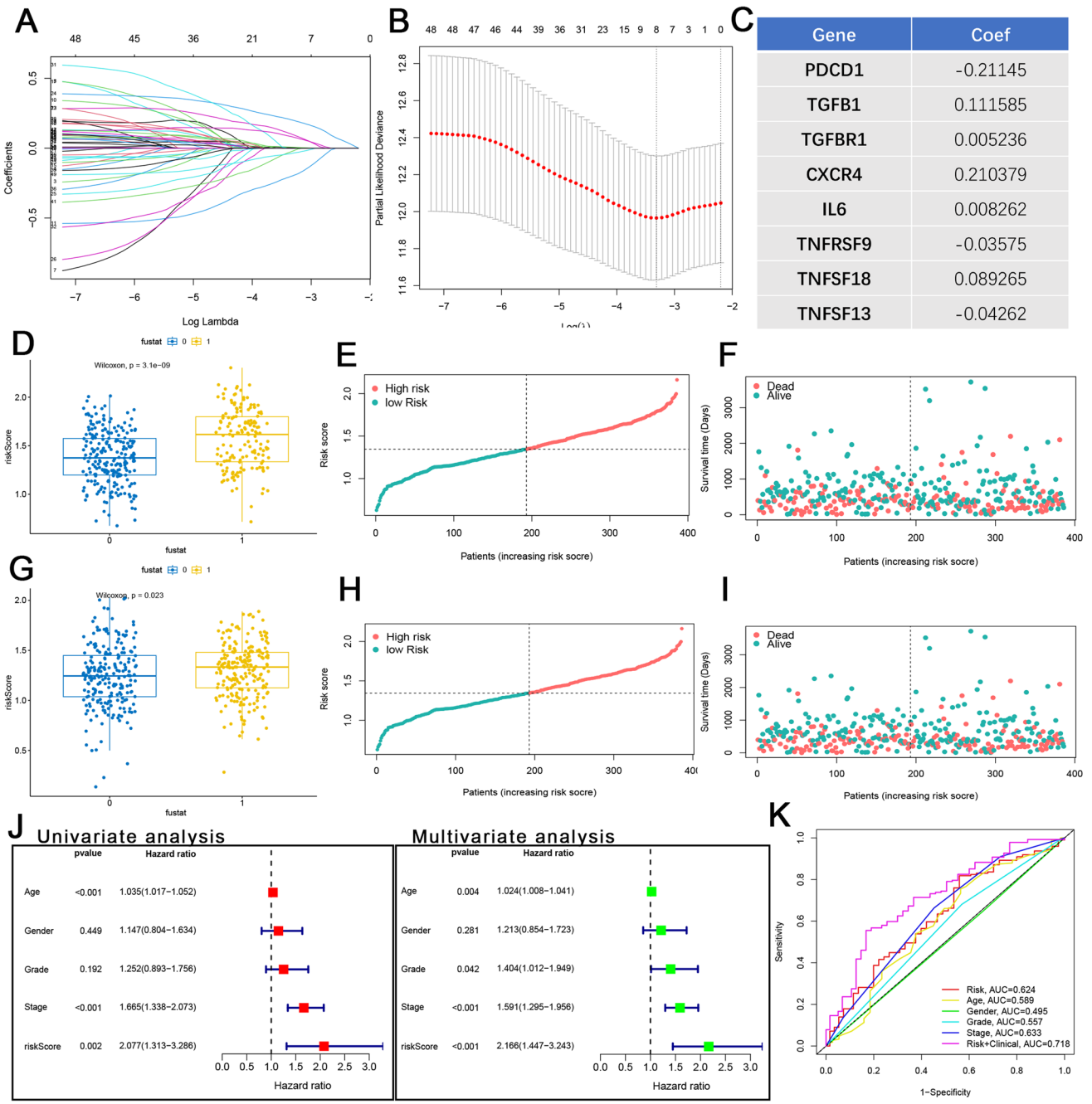

Fig. 5 SELP-associated immunomodulators in the prognosis of STAD. **A**, **B** LAASO coefficients of SELP-associated immunomodulator genes. **B** Identification of genes for prognostic risk models. **C** Identification of eight genes associated with prognosis. **D**–**F** Prognostic values of the risk scores in TCGA-STAD. **G**–**I** Prognostic values of the risk scores in GSE84437. **J** Univariate and multivariate Cox regression analyses with the risk score in STAD. **K** Receiver operating characteristic (ROC) curves of STAD prognostic factors

With the advancement of immunotherapy using immune checkpoint inhibitors (ICIs), the direction of gastric cancer treatment has changed clearly [35–37]. Although anti-PD-1/PD-L1 monotherapy has been approved as an advanced treatment, they are unlikely to be the first-line treatment for cancer [38, 39]. However, when combined with other therapies, ICIs have shown great potential for transforming clinical practice into a first-line treatment for advanced cancers [40]. However, most patients with advanced gastric cancer still do not benefit from immunotherapy [41]. With the development of precision medicine, biomarkers have been identified as effective therapies. Our search for effective biomarkers may be beneficial for immunotherapy.

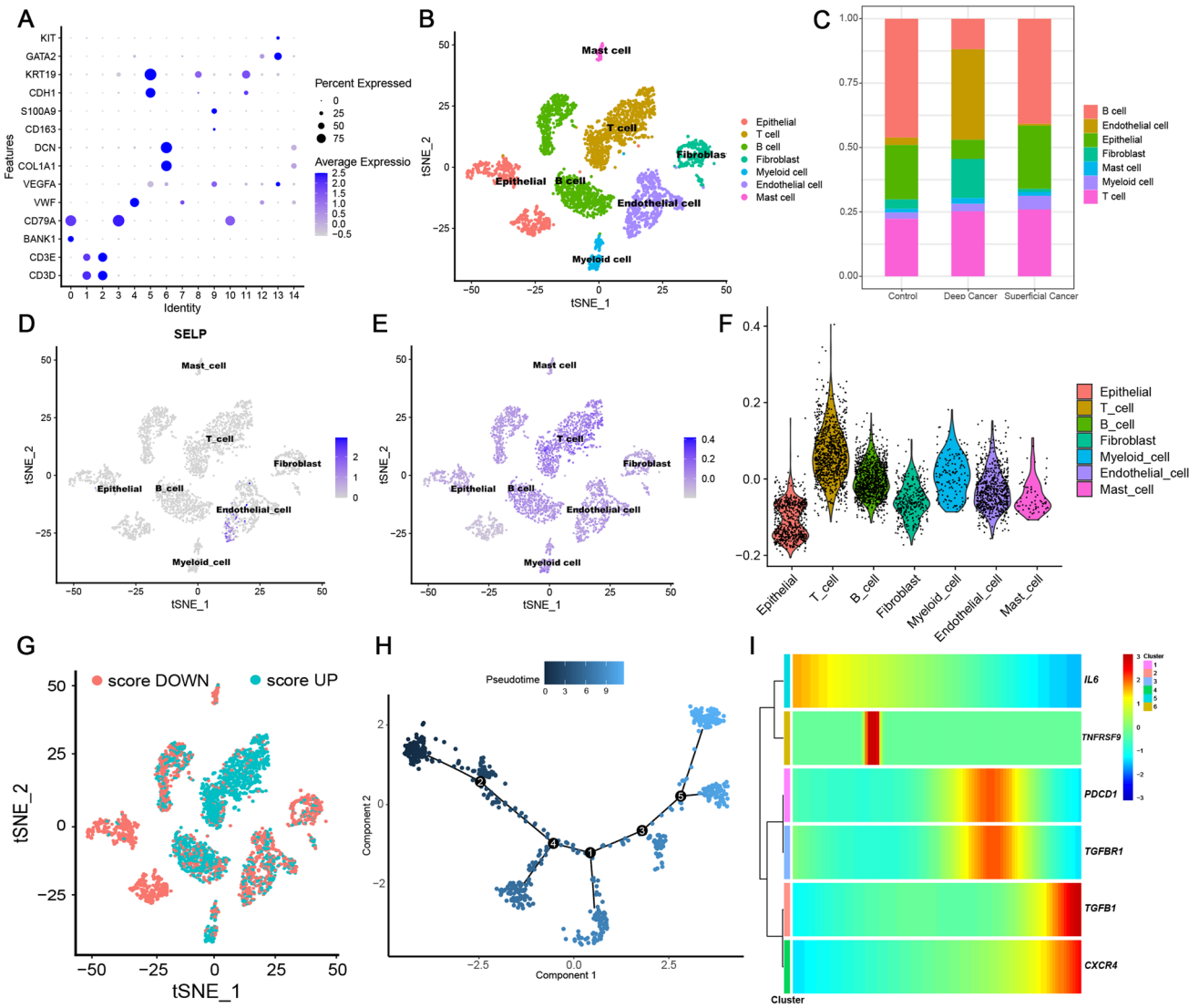

Fig. 6 Single-cell data analysis of GSE167297. **A** Manually annotated the cells. **B** Distribution of individual cells after annotation. Each cell population is represented by a different color. **C** The distribution of cells in normal tissues, deep cancer and pericancer. **D** Localization of the SELP gene in endothelial cells. **E**, **F** Distribution of SELP-associated immunomodulator genes associated with STAD prognosis in cells. **G** Volcano plot between groups with high and low SELP expression. **H** Unsupervised single-cell trajectory of endothelial cells with four branches. **I** Expression of genes at different times of endothelial cell development

In this study, a significant association between SELP expression and infiltration of tumor immune cells was observed in STAD. As a CAM, SELP is typically cross-linked with the P-selectin glycoprotein ligand-1 (PSGL-1) in the form of a dimer, thereby enhancing cell adhesion [42]. In addition to PSGL-1, CD44 and CD24 may also be functional ligands for SELP [43, 44]. SELP has been experimentally shown to be involved in a variety of immune processes, such as leukocyte recruitment and platelet activation [24, 45]. It has been demonstrated that SELP is involved in mediating myeloma macrophage-mediated drug resistance and is associated with TAM polarization [46, 47]. This study aimed to explore the potential role of SELP as a target molecule in the TME of gastric cancer.

First, we validated that SELP was associated with the clinical progression of STAD. CIBERSORT and ssGSEA were used to verify the correlation between SELP and immune-infiltrating cells in STAD. The results showed that many immune cells were positively correlated with SELP. Therefore, SELP may be related to macrophage polarization in the TME. At the same time, we analyzed the relationship between SELP and immune checkpoints, which suggested that high expression of SELP may be beneficial for immunotherapy and it also may be related to the involvement of SELP in normal immune function. Thus, SELP may play a dual role in gastric cancer by inhibiting survival and promoting cellular immunity. This illustrates the complexity of SELP in tumor immunity. At the next step, in order to further

Fig. 7 The SELP inhibitor KF38789 inhibits EMT in gastric cancer cells. **A** MKN-74 and MGC-803 cells were treated with KF38789 for 24, 48 ▶ and 72 h. Cell viability was determined by CCK-8 assay. **B** Colony formation density of KF38789-treated assessed by colony formation assay. **C** Statistics of colonies between control groups and KF38789-treated groups. **D**, **E** MKN-74 and MGC-803 were treated with KF38789 for 24 h, Changes in EMT proteins were observed by western blot, n = 3. **F** Wound healing assay results showed that compared with the control group, the migration of gastric cancer cells was significantly inhibited in KF38789 (Scale bar, 50 μM). **G** Statistics of wound healing assay. **H** The Transwell assay showed that the migration ability of gastric cancer cells was weakened under the treatment of KF compared with the control group (Scale bar, 100 μM). **I** Statistics of wound Transwell assay. (*P < 0.05, **P < 0.01, or ***P < 0.001)

explore the molecular mechanism of SELP in gastric cancer, we identified immunomodulators related to SELP. These results suggest that SELP plays an important role in the immune microenvironment during STAD progression.

In this study, LASSO regression was used to screen SELP-related immunomodulators associated with STAD prognosis. To further explore the mechanism of action of SELP and these SELP-related immunomodulators, we analyzed single-cell data from the GEO database. These results indicated that SELP may be associated with immunosuppression in gastric cancer. Moreover, the unsupervised single-cell trajectory of the SELP suggests that these immunomodulators play important roles at all stages of SELP development. The single-cell data results of this study provide evidence that SELP is a potential target for gastric cancer associated with the tumor immune microenvironment.

At the end of this study, we verified the inhibitory effect of SELP inhibitor KF38789 on EMT in gastric cancer cells, and the inhibitory effect is obvious. Several studies have confirmed that TME can affect EMT and the biology of gastric cancer cells [48]. In some tumors, integrins from the extracellular region influence EMT [49–51]. Therefore, we speculated that SELP may affect the invasion and migration of gastric cancer cells by regulating immune pathways.

In conclusion, our findings suggest that SELP plays a role in controlling the immune microenvironment in gastric cancer. The fundings may improve our understanding of gastric cancer and have the potential to lead to the development of advanced and strategies for gastric cancer therapy. Although, this experiment validates the feasibility of SELP as a potential therapeutic target for gastric cancer. The mechanism of SELP-mediated tumor immunity and the exact prognostic value of immune signatures should be further explored in the future, which is also a shortcoming of this study. In addition, most gastric cancers are not sensitive to immune checkpoint inhibitor monotherapy, so gastric cancer patients may require combination therapy to improve response to anti-PD-1 therapy or other ICIs. Therefore, if we can further explore the role of SELP in the immune microenvironment of gastric cancer, we can contribute to the evolving immunotherapy, and may also be combined with ICIs to achieve better clinical outcomes.

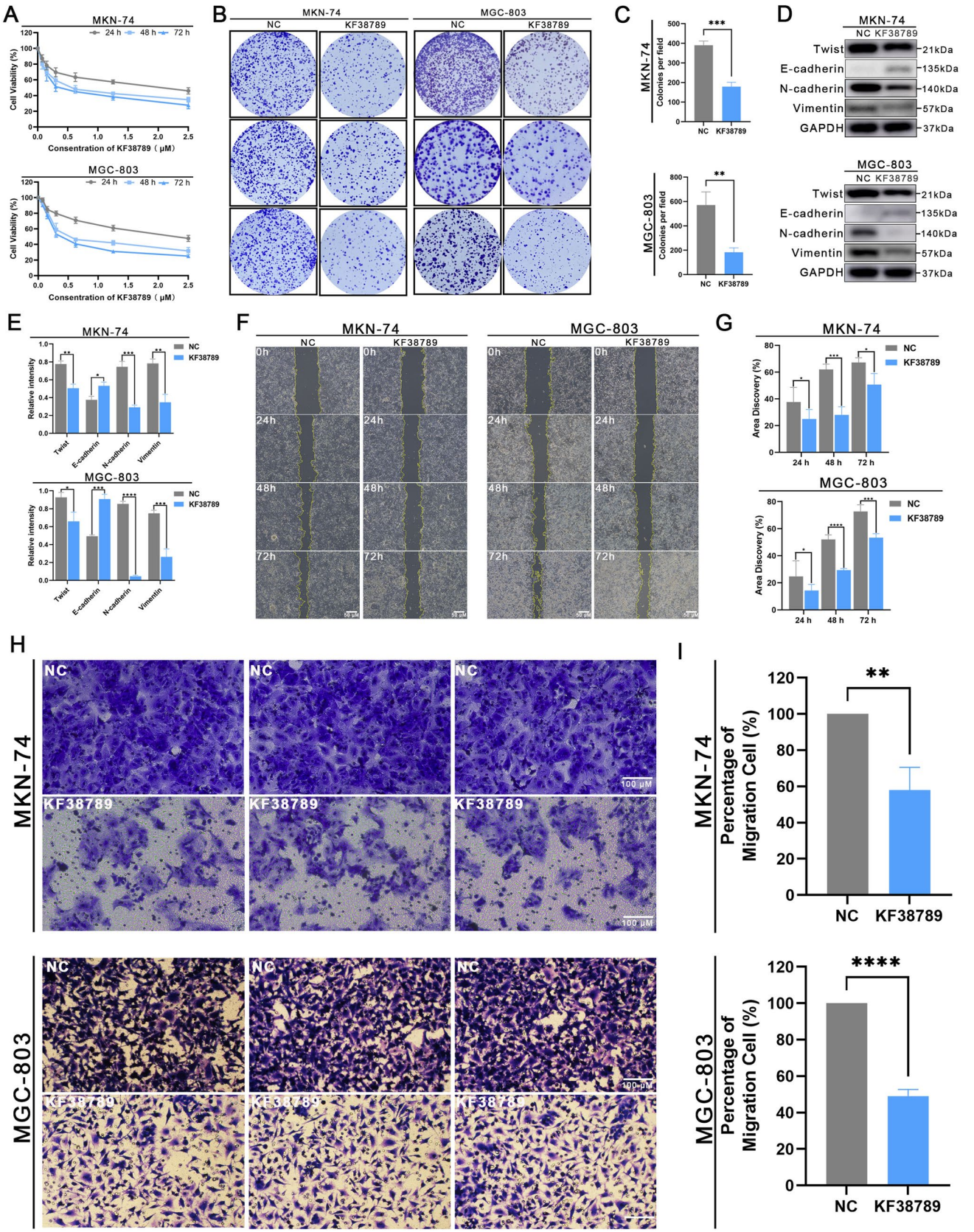
A
MKN-74
24 h
48 h
72 h
Cell Viability (%)
Consentration of KF38789 (μM)
MGC-803
B
MKN-74
MGC-803
NC
KF38789
C
MKN-74
Colonies per field
***
MGC-803
**
D
MKN-74
NC KF38789
Twist
E-cadherin
N-cadherin
Vimentin
GAPDH
21kDa
135kDa
140kDa
57kDa
37kDa
MGC-803
E
MKN-74
Relative intensity
Twist
E-cadherin
N-cadherin
Vimentin
MGC-803
F
MKN-74
MGC-803
0h
24h
48h
72h
G
MKN-74
Area Discovery (%)
MGC-803
H
MKN-74
MGC-803
100 μM
I
MKN-74
Percentage of Migration Cell (%)
**
MGC-803
****

Author contributions Y.W. and J.Y.L. contributed to the conception of the study and revised the manuscript. J.Y.L. performed the experiment and was a significant contributor to writing the manuscript. Y.W. contributed significantly to the analysis and put forward many constructive suggestions. Y.T. and X.X.L. performed the experiments, and X.B.Z and X.B.P. contributed significantly to the analysis. All authors have read and approved the final manuscript.

Funding This study was supported by grants from the Natural Science Foundation of China (Grant No. 82072707), Basic Research Project of Naval Medical University (Grant No. 2023MS023), Basic Medicine Research Fund (Grant No. 2023PY29).

Data availability Data is provided within the manuscript or supplementary information files.

Declarations

Consent for publication Not applicable.

Competing interests The authors declare no competing interests.

References

1. Siegel RL, Miller KD, Fuchs HE, Jemal A. Cancer statistics, 2021. Ca Cancer J Clin. 2021;71:7–33.
2. Sung H, Ferlay J, Siegel RL, Laversanne M, Soerjomataram I, Jemal A, Bray F. Global cancer statistics 2020: GLOBOCAN estimates of incidence and mortality worldwide for 36 cancers in 185 countries. CA Cancer J Clin. 2021;71:209–49.
3. Yang K, Lu L, Liu H, Wang X, Gao Y, Yang L, Li Y, Su M, Jin M, Khan S. A comprehensive update on early gastric cancer: defining terms, etiology, and alarming risk factors. Expert Rev Gastroenterol Hepatol. 2021;15:255–73.
4. Matsuoka T, Yashiro M. Novel biomarkers for early detection of gastric cancer. World J Gastroenterol. 2023;29:2515–33.
5. Hoft SG, Noto CN, DiPaolo RJ. Two distinct etiologies of gastric cancer: infection and autoimmunity. Front Cell Dev Biol. 2021;9: 752346.
6. Qiu H, Cao S, Xu R. Cancer incidence, mortality, and burden in China: a time-trend analysis and comparison with the United States and United Kingdom based on the global epidemiological data released in 2020. Cancer Commun. 2021;41:1037–48.
7. Yang L, Zheng R, Wang N, Yuan Y, Liu S, Li H, Zhang S, Zeng H, Chen W. Incidence and mortality of stomach cancer in China. Chin J Cancer Res. 2014;30(2018):291–8.
8. Etemadi A, Safiri S, Sepanlou SG, Ikuta K, Bisignano C, Shakeri R, Amani M, Fitzmaurice C, Nixon M, Abbasi N, Abolhassani H. The global, regional, and national burden of stomach cancer in 195 countries, 1990–2017: a systematic analysis for the Global Burden of Disease study 2017. Lancet Gastroenterol Hepatol. 2020;5:42–54.
9. Green PH, O'Toole KM, Slonim D, Wang T, Weg A. Increasing incidence and excellent survival of patients with early gastric cancer: experience in a United States medical center. Am J Med. 1988;85:658–61.
10. Hida K, Maishi N, Annan DA, Hida Y. Contribution of tumor endothelial cells in cancer progression. Int J Mol Sci. 2018;19:1272.
11. de Visser KE, Joyce JA. The evolving tumor microenvironment: from cancer initiation to metastatic outgrowth. Cancer Cell. 2023;41:374–403.
12. Park J, Hsueh PC, Li Z, Ho PC. Microenvironment-driven metabolic adaptations guiding CD8(+) T cell anti-tumor immunity. Immunity. 2023;56:32–42.
13. Gonzalez H, Hagerling C, Werb Z. Roles of the immune system in cancer: from tumor initiation to metastatic progression. Genes Dev. 2018;32:1267–84.
14. Khalaf K, Hana D, Chou JT, Singh C, Mackiewicz A, Kaczmarek M. Aspects of the tumor microenvironment involved in immune resistance and drug resistance. Front Immunol. 2021;12: 656364.
15. Petitprez F, Meylan M, de Reyniès A, Sautès-Fridman C, Fridman WH. The tumor microenvironment in the response to immune checkpoint blockade therapies. Front Immunol. 2020;11:784.
16. Guven DC, Sahin TK, Erul E, Rizzo A, Ricci AD, Aksoy S, Yalcin S. The association between albumin levels and survival in patients treated with immune checkpoint inhibitors: a systematic review and meta-analysis. Front Mol Biosci. 2022;9:1039121.
17. Rizzo A, Mollica V, Tateo V, Tassinari E, Marchetti A, Rosellini M, De Luca R, Santoni M, Massari F. Hypertransaminasemia in cancer patients receiving immunotherapy and immune-based combinations: the MOUSEION-05 study. Cancer Immunol Immunother. 2023;72:1381–94.
18. Dall'Olio FG, Rizzo A, Mollica V, Massucci M, Maggio I, Massari F. Immortal time bias in the association between toxicity and response for immune checkpoint inhibitors: a meta-analysis. Immunotherapy. 2021;13:257–70.
19. Cao T, Zhang W, Wang Q, Wang C, Ma W, Zhang C, Ge M, Tian M, Yu J, Jiao A, Wang L, Liu M, Wang P, Guo Z, Zhou Y, Chen S, Yin W, Yi J, Guo H, Han H, Zhang B, Wu K, Fan D, Wang X, Nie Y, Lu Y, Zhao X. Cancer SLC6A6-mediated taurine uptake transactivates immune checkpoint genes and induces exhaustion in CD8(+) T cells. Cell. 2024;187:2288-2304.e2227.

20. Kim ST, Cristescu R, Bass AJ, Kim KM, Odegaard JI, Kim K, Liu XQ, Sher X, Jung H, Lee M, Lee S, Park SH, Park JO, Park YS, Lim HY, Lee H, Choi M, Talasaz A, Kang PS, Cheng J, Loboda A, Lee J, Kang WK. Comprehensive molecular characterization of clinical responses to PD-1 inhibition in metastatic gastric cancer. Nat Med. 2018;24:1449–58.
21. Samstein RM, Lee CH, Shoushtari AN, Hellmann MD, Shen R, Janjigian YY, Barron DA, Zehir A, Jordan EJ, Omuro A, Kaley TJ, Kendall SM, Motzer RJ, Hakimi AA, Voss MH, Russo P, Rosenberg J, Iyer G, Bochner BH, Bajorin DF, Al-Ahmadie HA, Chaft JE, Rudin CM, Riely GJ, Baxi S, Ho AL, Wong RJ, Pfister DG, Wolchok JD, Barker CA, Gutin PH, Brennan CW, Tabar V, Mellinghoff IK, DeAngelis LM, Ariyan CE, Lee N, Tap WD, Gounder MM, D'Angelo SP, Saltz L, Stadler ZK, Scher HI, Baselga J, Razavi P, Klebanoff CA, Yaeger R, Segal NH, Ku GY, DeMatteo RP, Ladanyi M, Rizvi NA, Berger MF, Riaz N, Solit DB, Chan TA, Morris LGT. Tumor mutational load predicts survival after immunotherapy across multiple cancer types. Nat Genet. 2019;51:202–6.
22. Ma X, Jia S, Wang G, Liang M, Guo T, Du H, Li S, Li X, Huangfu L, Guo J, Xing X, Ji J. TRIM28 promotes the escape of gastric cancer cells from immune surveillance by increasing PD-L1 abundance. Signal Transduct Target Ther. 2023;8:246.
23. Yeini E, Satchi-Fainaro R. The role of P-selectin in cancer-associated thrombosis and beyond. Thromb Res. 2022;213(Suppl 1):S22-s28.
24. Borsig L. Selectins in cancer immunity. Glycobiology. 2018;28:648–55.
25. Yoshihara K, Shahmoradgoli M, Martínez E, Vegesna R, Kim H, Torres-Garcia W, Treviño V, Shen H, Laird PW, Levine DA, Carter SL, Getz G, Stemke-Hale K, Mills GB, Verhaak RG. Inferring tumour purity and stromal and immune cell admixture from expression data. Nat Commun. 2013;4:2612.
26. Robinson MD, McCarthy DJ, Smyth GK. edgeR: a bioconductor package for differential expression analysis of digital gene expression data. Bioinformatics. 2010;26:139–40.
27. Newman AM, Liu CL, Green MR, Gentles AJ, Feng W, Xu Y, Hoang CD, Diehn M, Alizadeh AA. Robust enumeration of cell subsets from tissue expression profiles. Nat Methods. 2015;12:453–7.
28. Bindea G, Mlecnik B, Tosolini M, Kirilovsky A, Waldner M, Obenauf AC, Angell H, Fredriksen T, Lafontaine L, Berger A, Bruneval P, Fridman WH, Becker C, Pagès F, Speicher MR, Trajanoski Z, Galon J. Spatiotemporal dynamics of intratumoral immune cells reveal the immune landscape in human cancer. Immunity. 2013;39:782–95.
29. Ru B, Wong CN, Tong Y, Zhong JY, Zhong SSW, Wu WC, Chu KC, Wong CY, Lau CY, Chen I, Chan NW, Zhang J. TISIDB: an integrated repository portal for tumor-immune system interactions. Bioinformatics. 2019;35:4200–2.
30. Liao Y, Wang J, Jaehnig EJ, Shi Z, Zhang B. WebGestalt 2019: gene set analysis toolkit with revamped UIs and APIs. Nucleic Acids Res. 2019;47:W199-w205.
31. Wu TT, Chen YF, Hastie T, Sobel E, Lange K. Genome-wide association analysis by lasso penalized logistic regression. Bioinformatics. 2009;25:714–21.
32. Butler A, Hoffman P, Smibert P, Papalexi E, Satija R. Integrating single-cell transcriptomic data across different conditions, technologies, and species. Nat Biotechnol. 2018;36:411–20.
33. Patel KD, Cuvelier SL, Wiehler S. Selectins: critical mediators of leukocyte recruitment. Semin Immunol. 2002;14:73–81.
34. Chen Y, Jia K, Sun Y, Zhang C, Li Y, Zhang L, Chen Z, Zhang J, Hu Y, Yuan J, Zhao X, Li Y, Gong J, Dong B, Zhang X, Li J, Shen L. Predicting response to immunotherapy in gastric cancer via multi-dimensional analyses of the tumour immune microenvironment. Nat Commun. 2022;13:4851.
35. Li S, Yu W, Xie F, Luo H, Liu Z, Lv W, Shi D, Yu D, Gao P, Chen C, Wei M, Zhou W, Wang J, Zhao Z, Dai X, Xu Q, Zhang X, Huang M, Huang K, Wang J, Li J, Sheng L, Liu L. Neoadjuvant therapy with immune checkpoint blockade, antiangiogenesis, and chemotherapy for locally advanced gastric cancer. Nat Commun. 2023;14:8.
36. Takei S, Kawazoe A, Shitara K. The new era of immunotherapy in gastric cancer. Cancers. 2022;14:1054.
37. Kong J, Ha D, Lee J, Kim I, Park M, Im SH, Shin K, Kim S. Network-based machine learning approach to predict immunotherapy response in cancer patients. Nat Commun. 2022;13:3703.
38. Zhang H, Liu L, Liu J, Dang P, Hu S, Yuan W, Sun Z, Liu Y, Wang C. Roles of tumor-associated macrophages in anti-PD-1/PD-L1 immunotherapy for solid cancers. Mol Cancer. 2023;22:58.
39. Chu X, Tian W, Wang Z, Zhang J, Zhou R. Co-inhibition of TIGIT and PD-1/PD-L1 in cancer immunotherapy: mechanisms and clinical trials. Mol Cancer. 2023;22:93.
40. Li K, Zhang A, Li X, Zhang H, Zhao L. Advances in clinical immunotherapy for gastric cancer. Biochimica et biophysica acta Rev Cancer. 2021;1876: 188615.
41. Moehler M, Dvorkin M, Boku N, Özgüroğlu M, Ryu MH, Muntean AS, Lonardi S, Nechaeva M, Bragagnoli AC, Cos kun HS, Cubillo Gracian A, Takano T, Wong R, Safran H, Vaccaro GM, Wainberg ZA, Silver MR, Xiong H, Hong J, Taieb J, Bang YJ. Phase III trial of avelumab maintenance after first-line induction chemotherapy versus continuation of chemotherapy in patients with gastric cancers: results from JAVELIN gastric 100. J Clin Oncol. 2021;39:966–77.
42. Ramachandran V, Yago T, Epperson TK, Kobzdej MM, Nollert MU, Cummings RD, Zhu C, McEver RP. Dimerization of a selectin and its ligand stabilizes cell rolling and enhances tether strength in shear flow. Proc Natl Acad Sci USA. 2001;98:10166–71.
43. Barthel SR, Gavino JD, Descheny L, Dimitroff CJ. Targeting selectins and selectin ligands in inflammation and cancer. Expert Opin Ther Targets. 2007;11:1473–91.
44. Aigner S, Sthoeger ZM, Fogel M, Weber E, Zarn J, Ruppert M, Zeller Y, Vestweber D, Stahel R, Sammar M, Altevogt P. CD24, a mucin-type glycoprotein, is a ligand for P-selectin on human tumor cells. Blood. 1997;89:3385–95.
45. McEver RP. Selectins: initiators of leucocyte adhesion and signalling at the vascular wall. Cardiovasc Res. 2015;107:331–9.
46. Zheng Y, Yang J, Qian J, Qiu P, Hanabuchi S, Lu Y, Wang Z, Liu Z, Li H, He J, Lin P, Weber D, Davis RE, Kwak L, Cai Z, Yi Q. PSGL-1/selectin and ICAM-1/CD18 interactions are involved in macrophage-induced drug resistance in myeloma. Leukemia. 2013;27:702–10.
47. Tchernychev B, Furie B, Furie BC. Peritoneal macrophages express both P-selectin and PSGL-1. J Cell Biol. 2003;163:1145–55.
48. Xu J, Lamouille S, Derynck R. TGF-beta-induced epithelial to mesenchymal transition. Cell Res. 2009;19:156–72.

49. Helal-Neto E, Brandão-Costa RM, Saldanha-Gama R, Ribeiro-Pereira C, Midlej V, Benchimol M, Morandi V, Barja-Fidalgo C. Priming endothelial cells with a melanoma-derived extracellular matrix triggers the activation of αvβ3/VEGFR2 Axis. J Cell Physiol. 2016;231:2464–73.
50. Cichon MA, Radisky DC. Extracellular matrix as a contextual determinant of transforming growth factor-β signaling in epithelial-mesenchymal transition and in cancer. Cell Adh Migr. 2014;8:588–94.
51. Li M, Wang Y, Li M, Wu X, Setrerrahmane S, Xu H. Integrins as attractive targets for cancer therapeutics. Acta pharmaceutica Sinica B. 2021;11:2726–37.